AD-A066 083　INDIANA UNIV AT BLOOMINGTON DEPT OF CHEMISTRY　F/G 7/2
COMPARISON OF ATOMIC FLUORESCENCE POWER EFFICIENCIES FOR THE HE--ETC(U)
MAR 79　K A SATURDAY, G M HIEFTJE　N00014-76-C-0838
UNCLASSIFIED　TR-23　NL

1 OF 1
ADA
066083

END
DATE
FILMED
5 79
DDC

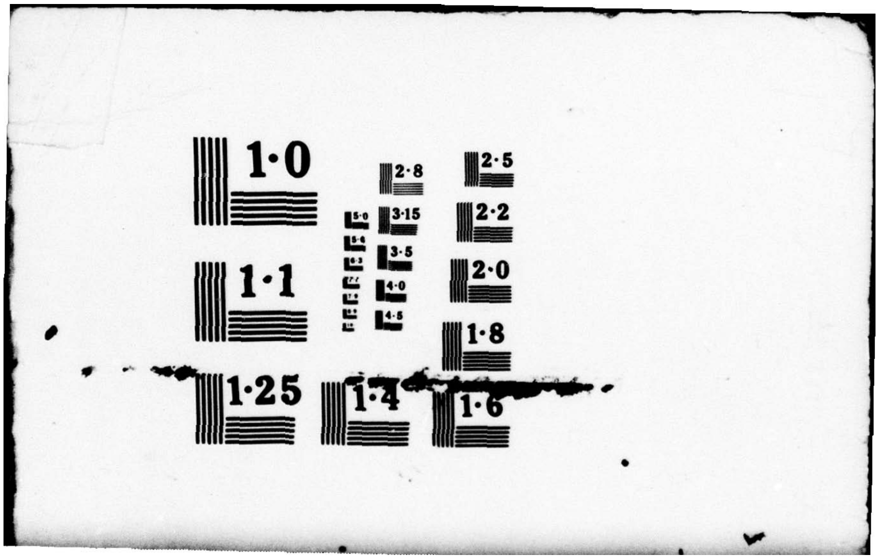
1·0
2·8
2·5
5·0
3·15
2·2
3·5
1·1
2·0
4·0
4·5
1·8
1·25
1·4
1·6

LEVEL II

⑫

AD A0 66083

DDC FILE COPY

SECURITY CLASSIFICATION OF THIS PAGE (When Data Entered)

REPORT DOCUMENTATION PAGE

READ INSTRUCTIONS BEFORE COMPLETING FORM

1. REPORT NUMBER: EIGHTEEN
2. GOVT ACCESSION NO.
3.

4. TITLE (and Subtitle): ⑥ Comparison of Atomic Fluorescence Power Efficiencies for the Helium-Oxygen-Acetylene and Air-Acetylene Flames.

5. TYPE OF REPORT & PERIOD COVERED: ⑨ Interim Technical Report,

6. PERFORMING ORG. REPORT NUMBER: 23

7. AUTHOR(s): ⑩ K. A. Saturday ~~and~~ G. M. Hieftje

8. CONTRACT OR GRANT NUMBER(s): N14-76-C0838

9. PERFORMING ORGANIZATION NAME AND ADDRESS:
Department of Chemistry
Indiana University
Bloomington, IN 47405

10. PROGRAM ELEMENT, PROJECT, TASK AREA & WORK UNIT NUMBERS: NR 051-622

11. CONTROLLING OFFICE NAME AND ADDRESS: ⑪ 5 Mar 79

12. REPORT DATE: March 5, 1979

13. NUMBER OF PAGES: 41

14. MONITORING AGENCY NAME & ADDRESS (if different from Controlling Office):
Office of Naval Research
Washington, D. C.
⑫ 41 p.

15. SECURITY CLASS. (of this report): Unclassified

15a. DECLASSIFICATION/DOWNGRADING SCHEDULE

16. DISTRIBUTION STATEMENT (of this Report)

Approved for public release; distribution unlimited

⑭ TR-23, 18

17. DISTRIBUTION STATEMENT (of the abstract entered in Block 20, if different from Report)

Prepared for publication in ANALYTICAL CHEMISTRY

DDC
RECEIVED
MAR 20 1979
D

18. SUPPLEMENTARY NOTES

⑮ N00014-76-C-0838,
NSF-CHE77-22152

19. KEY WORDS (Continue on reverse side if necessary and identify by block number)

Flame spectrometry, quantum efficiency, atomic absorption, atomic fluorescence

20. ABSTRACT (Continue on reverse side if necessary and identify by block number)

Power efficiencies for five elements have been measured for the helium-oxygen-acetylene and air-acetylene flames. The increased power efficiencies found in this study for the helium-diluted flame, coupled with its enhanced atom formation capabilities, suggest that greater atomic fluorescence sensitivity should exist. However, in a comparison study with an air-acetylene flame using identical experimental conditions, a decreased atomic fluorescence signal-to-noise ratio was found for most elements in the helium-diluted flame. This decrease has been ascribed to greater background

over

DD FORM 1 JAN 73 1473 EDITION OF 1 NOV 65 IS OBSOLETE
S/N 0102-014-6601

Unclassified
SECURITY CLASSIFICATION OF THIS PAGE (When Data Entered)

79 03 19 070

176 685

20. continued

emission noise in the higher-temperature helium-diluted flame and decreased nebulization efficiency caused by the low density of the helium-containing nebulizer gas. A comparison of flame emission detection limits for the two flames indicates the increased sensitivity of the higher-temperature helium-acetylene flame, despite its lower nebulization efficiency.

Comparison of Atomic Fluorescence Power Efficiencies for the Helium-Oxygen-Acetylene and Air-Acetylene Flames

K. A. Saturday and G. M. Hieftje*
Department of Chemistry
Indiana University
Bloomington, Indiana 47401

BRIEF

Fluorescence power efficiencies were measured for five elements in the helium-oxygen-acetylene and air-acetylene flames and revealed a distinct radiant power conversion increase for the helium-diluted flame.

ABSTRACT

Power efficiencies for five elements have been measured for the helium-oxygen-acetylene and air-acetylene flames. The increased power efficiencies found in this study for the helium-diluted flame, coupled with its enhanced atom formation capabilities, suggest that greater atomic fluorescence sensitivity should exist. However, in a comparison study with an air-acetylene flame using identical experimental conditions, a decreased atomic fluorescence signal-to-noise ratio was found for most elements in the helium-diluted flame. This decrease has been ascribed to greater background emission noise in the higher-temperature helium-diluted flame and decreased nebulization efficiency caused by the low density of the helium-containing nebulizer gas. A comparison of flame emission detection limits for the two flames indicates the increased sensitivity of the higher-temperature helium-oxygen-acetylene flame, despite its lower nebulization efficiency.

Studies of the physical characteristics (1) and atom formation properties (2) of the helium-oxygen-acetylene flame have suggested its application to atomic fluorescence spectrometry. The properties of the helium-diluted flame correlate well with those required of an ideal atomic fluorescence flame cell (3, 4). Among these properties are:

a) high desolvation and atomization efficiencies,

b) low background emission,

c) high stability and

d) low concentrations of quenching species.

The helium-oxygen-acetylene flame was initially studied because of its atom formation capabilities (5). In that study, the desolvation rates of individual droplets injected into a flame were measured; it was found that replacing the nitrogen component of an air-acetylene flame with helium doubled the rate of droplet desolvation. Because of this increased rate of desolvation, a greater fraction of sample is available for atomic spectrometric analysis and the number of large undesolvated droplets, which can scatter incident radiation, is reduced. A recent study measured the atom formation efficiency of the helium-oxygen-acetylene flame and showed the flame to possess atom formation capabilities between those of two commonly used atom cells, the nitrous oxide-acetylene and air-acetylene flames (2).

The background emission spectrum of the helium-oxygen-acetylene flame is similar to that of the air-acetylene flame (1). Although the strongest feature in the spectrum of the helium-diluted flame (the OH band at 310 nm) is four times more intense than in the air-sustained flame, neither flame exhibits a background as intense or complex as that of the nitrous oxide-acetylene mixture.

Improvements in burner design have increased the stability of the helium-oxygen-acetylene flame (1, 2). The first study employing this flame gas mixture showed that the helium-diluted flame could not be safely supported on burners constructed for air-acetylene or nitrous oxide-acetylene combustion (5). However, simple modifications to existing burners allowed the physical characterization of the flame (2); further developments in burner construction have permitted the flame to be utilized with a commercial nebulization chamber, resulting in safe and reproducible performance (2).

The quenching environment of the helium-oxygen-acetylene flame should be favorable, because helium is the principal flame constituent. Other workers have measured the quenching effects of helium, nitrogen, argon and other species on the atomic fluorescence of several metal atoms in flames (6-9). Helium was found to possess a smaller quenching cross section than nitrogen (.1 Å^2 compared to 6.5 Å^2), and was comparable to argon. Because of the low quenching cross-section of helium, an increased fluorescence yield should occur for a helium-containing flame. Verification of this hypothesis is the subject of the present investigation.

Although the characteristics of the helium-oxygen-acetylene flame correlate well with those of the ideal atomic fluorescence atom cell, it has never been employed in fluorescence measurements. In the present study, the helium-diluted flame is compared to the air-acetylene flame in its quenching characteristics. Specifically, fluorescence power efficiencies are measured in both flames. It was found that power efficiencies for the helium-diluted flame were greater, but atomic fluorescence signal-to-noise ratios were not greatly improved, because of the decreased nebulization efficiency of the helium-containing nebulization gas and the increased background emission noise of the flame. In contrast, emission measurements exhibit lower detection limits, primarily because of the higher temperature of the helium-sustained flame.

EXPERIMENTAL

Burner. The construction of the capillary burner used in this study has been previously described (2). However, a component used to support an inert-gas sheath has been added to the burner assembly. The design of this component is similar to one previously described (10) and was constructed from 18-gauge capillary needles (Popper and Sons, Inc., New Hyde Park, N.Y.) using the same procedure followed for the burner head construction (2). The resulting gas-sheath capillary array fits snugly around the burner head and contains 212 exit ports arranged in four concentric circles to provide sufficient sheathing for the flame.

Instrumental System. A schematic diagram of the optical system used for the determination of fluorescence power efficiencies is shown in Figure 1; a detailed list of the optical components, detection equipment and experimental conditions is contained in Table I. In the described experimental system, the output of the continuum light source was focussed into the center of the flame by lens, L1. Diaphragm D2 formed the limiting aperture for the external optical system, while D1 served to reduce the amount of stray light present.

For the measurement of absorption and fluorescence signals, equivalent optical systems were constructed to focus either the continuum source or fluorescence radiation onto the appropriate monochromator entrance slit. Although identical components were used for each of the detection portions of the system, the equivalence of their optical performance could not be assumed. To assess their similarity, the magnification produced by each lens, L2 and L3, was measured. In the absorption portion of the system, the continuum source was focussed at the center of the burner, and the size of the images produced both at the burner and the monochromator entrance slit were determined. For the fluorescence system, a front surface mirror was placed at the focus of L1, in place of the burner, to divert the light beam into the fluorescence portion of the system. Again, the size of both images was determined. The measurements of image size were made by placing a screen at appropriate positions in the optical system and determining the size of the images on the screen with calipers. Magnifications computed from the results of these measurements agreed to within 5% , indicating a high degree of similarity in the two optical trains. Any differences in throughput for the two lenses will be considered in the calibration of the detector responses described below.

<u>Solutions</u>. Stock solutions were prepared according to standard methods (11) with reagent grade chemicals and distilled, deionized water. Successive dilutions yielded solutions

in the proper concentration range for this study.

Determination of Fluorescence Power Efficiency

Fluorescence power efficiencies for atoms in flames are equal to the ratio of the fluorescence intensity to the amount of radiation absorbed from the external excitation source (6-9, 12-16). For a measurement system employing a monochromator and a continuum source, the following relationship for fluorescence power yields, Y_P, has been derived (12):

$$Y_P = \left(\frac{I_F}{\Delta I_A}\right)\left(\frac{W_A H_A}{W_F H_F}\right)\left(\frac{4\pi}{\Omega}\right)\left(\frac{A_F}{A_S}\right)\left(\frac{D_F}{D_A}\right) \qquad (1)$$

In equation 1, I_F is the measured fluorescence signal; ΔI_A is the difference in signals recorded for the absorption measurement (i.e. the difference between the signals obtained with and without atoms present in the flame) after a correction for the transmission of the neutral density filter was applied. W_A, H_A, W_F and H_F are the width and height of the entrance slits of the absorption and fluorescence monochromators, respectively. The solid angle of radiation incident on the absorption monochromator is given by Ω, whereas A_F denotes the illuminated area of the flame from which fluorescence is emitted. A_S is the illuminated area at the slit of the absorption monochromator.

Corrections for differences in detector response and optical system throughput are denoted by D_A and D_F; the quantities $I_F D_F$ and $\Delta I_A D_A$ represent the corrected values of fluorescence and absorption intensity. Values for these parameters are listed in Table 2; their determination is described below.

Evaluation of Experimental Parameters. The entrance slit height of both monochromators (H_F and H_A) was kept constant at 5mm. The ratio of the slit widths (W_A/W_F) was approximated by measuring the ratio of the spectral bandpasses of the monochromators at the slit-width settings used in the power efficiency determination. The spectral bandpasses were measured by scanning over a hollow cathode emission line and determining the width at the half-peak-intensity point of the wavelength trace. Spectral bandpasses determined by this method agreed to within one percent with the ratio of peak area to peak intensity of the hollow cathode wavelength scan. The spectral bandpasses of the absorption and fluorescence monochromators were found to be 0.16 and 0.87 nm, respectively, giving an approximated slit width ratio of 5.4. For this approximation to be valid, the reciprocal linear dispersion of the two similar monochromators must be identical, a condition which is probably met. Regardless, selection of the proper conditions for determination of the relative detector response will cause this spectral bandpass factor to disappear from equation 1 (See Appendix A).

The solid angle of radiation incident on the monochromator, Ω, was calculated as the ratio of the illuminated area of lens L2 to the square of its distance from the absorption monochromator slit. The present system was found to intercept 0.021 steradians of the fluorescence intensity, which is larger than the 0.019 steradian acceptance angle of the monochromator. An assumption made in the derivation of equation 1 requires Ω to be larger than the monochromator acceptance angle; the present instrument meets this condition. The relative error in the solid angle determination is estimated to be 4%.

A_S, the area which is illuminated by the continuum source at the entrance slit of the absorption monochromator is determined directly. With the Eimac arc lamp, a diffuse circular image of the arc is produced at the monochromator (17). The 0.48 cm^2 illuminated area of this image was measured by placing a focussing screen in the plane of the monochromator entrance slits, and measuring the image size either photographically, or visually with calipers. Results of both methods agree to within 5%.

The area of fluorescence in the flame, A_F, can be approximated as the product of the flame width and the height of the image of the excitation source at the center of the flame (12).

The approximation, however, assumes the light is collimated as it passes through the flame. For the system employed in this study, the height of the images remains fairly constant throughout the width of the flame at 1.0 cm ± 0.1 cm. A slight increase in image height is observed near the flame edge. The widths of the sheathed air-acetylene and helium-oxygen-acetylene flames were determined to be 1.0 ± 0.1 cm and 1.5 + 0.1 cm respectively at a height of 1 cm above the top of the primary reaction zone. Flame widths were determined by measuring the photographic image of a sodium-containing flame. Details concerning the flame width measurement technique can be found elsewhere (2). The observation height (1 cm above the primary reaction zone) was selected on the basis of previous studies (2) employing the same burner/nebulizer system, which showed that region to contain the maximum atom concentration for several elements.

To correct for differences in absorption and fluorescence detector response, the ratio of D_F to D_A was determined rather than the absolute sensitivity of each detector. In the calibration procedure, the responses for both the absorption and fluorescence detectors were measured when the output of a stable continuum source (the Eimac lamp) was directed into each of the monochromators. A front-surface mirror was placed at the focus of lens L1 instead of the burner as shown in Figure 1, and served to direct the continuum radiation into the fluorescence monochromator. This mirror was removed for the measurement of the absorption detector responses. To avoid overloading the photomultiplier tubes, a 0.1% T neutral-density filter (see Table 1) was placed immediately after lens L1 instead of directly before the absorption monochromator.

The factor D_F/D_A in equation 1 was calculated by ratioing the responses of the fluorescence and absorption detectors, obtained with the procedure outlined above. Separate factors were measured for the relative detector response at each of the wavelengths employed in the power efficiency determinations. For each measurement, the monochromator entrance slit height and width were kept constant at the settings listed in Table 2. Appendix A describes in more detail the validity of this method.

Experimental Procedure. To evaluate equation 1, both fluorescence and absorption measurements must be made for each element being studied. The ratio of fluorescence intensity to absorbed continuum source radiation was evaluated by recording peak values for both the absorption and fluorescence signals at the wavelength of a particular transition for each element. To obtain these peak values, the monochromators were scanned over the wavelength region of the transition and stopped at the wavelength of maximum absorption or fluorescence. Multiple determinations of the fluorescence and absorption signals were then obtained. For the fluorescence measurements, it was found that no correction for scattered radiation was required.

In order to correct for self-absorption effects in the calculated power efficiency value (6, 15, 16), data were collected over a range of solution concentrations for all elements, and a power efficiency value was calculated for each analyte concentration. These concentration-dependent power efficiency values were then extrapolated to zero concentration to obtain the final reported power efficiencies.

Signal-to-Noise Studies. To assess the utility of the helium-diluted flame in both emission and fluorescence atomic spectrometry, signal-to-noise studies were performed for several elements. For atomic fluorescence, signal-to-noise ratios were measured in the helium-oxygen-acetylene and air-acetylene flames for 10 μg mL^{-1} solutions of six elements. This procedure was selected in order to compare the values for the helium-containing flame with those for the argon-oxygen-acetylene flame obtained with a similar method (4). For all determinations, a nebulization rate of 2 mL min^{-1} and a 3 s time constant were employed. The signal-to-noise ratio for zinc fluorescence was included in this study, although a power efficiency could not be determined for that element because of the low sensitivity of the absorption detector system at the 213.8 nm zinc resonance line.

For atomic emission, detection limits for six elements were determined in both the air-acetylene and helium-oxygen-acetylene flames, using previously described methods (18). A 100 ms time constant and a 2 mL min^{-1} nebulization rate were employed for both flames. No attempt was made to optimize conditions for the best detection limit values.

RESULTS AND DISCUSSION

Power Efficiency Measurements. Power efficiencies for five elements, obtained in both the air-acetylene and helium-oxygen-acetylene flames, are listed in Table 3. Because resonance transitions were employed for all elements, these values also represent the quantum efficiencies for the transitions (19). The average relative standard deviation for the values is 10%, most of which arises from variation in the fluorescence to absorption intensity ratio, possibly caused by nebulizer drift.

The increases in power efficiency observed here upon substitution of helium for nitrogen are similar to those reported by Jenkins (20) in studies on nitrogen-, helium- and argon-diluted oxygen-hydrogen flames. Ten-fold improvements in power efficiencies were also observed when argon was substituted for nitrogen in a flame-sheathed hydrogen-oxygen-nitrogen flame (13). This finding suggests that even further increases in power efficiency might be possible for the helium-oxygen-acetylene flame if a sheath flame were used instead of the inert gas sheath employed in the present study.

In Table 3, power efficiencies for the helium-diluted flame are ratioed to those obtained in the air-acetylene flame. Significantly, the ratio for chromium is higher than that for any other element tested. Johnson and Winefordner (4) measured a similar improvement in signal-to-noise ratio for chromium over that for iron, magnesium and copper when an argon-oxygen-acetylene and air-acetylene flame were compared. The findings of the present study suggest that this improvement is caused by an increased fluorescence power efficiency, although an increased atom formation efficiency (postulated by the previous workers) might also contribute to the improvement. No firm reason for the increased power efficiency of Cr has been established.

The increases in fluorescence power efficiency for the helium-oxygen-acetylene flame (cf. Table 3) suggest that analytical sensitivity might be improved using this flame. Sensitivity increases can be examined through use of a growth curve. Figure 2 shows an analytical growth curve for copper in both the air-acetylene and helium-oxygen-acetylene flames. The increased fluorescence produced in the helium-diluted flame can be attributed directly to improved power efficiency, because it is known that copper free atom fractions are approximately the same in both flames (2).

Fluorescence Intensity Measurements. In the measurements portrayed by Figure 2, the same nebulizer was employed for both the helium-oxygen- and air-fed flames. Unfortunately, the nebulizer was optimized for air usage, and further improvements should be realizable through nebulizer redesign. In fact, previous studies have shown the nebulization efficiency for the present experimental system to be 16.5% for an air-acetylene flame, but only 9.9% for the helium-oxygen-acetylene flame (2). This reduced efficiency results in 40% less sample being introduced into the helium-diluted flame. This fact, coupled with the larger dilution of the atomic species in the increased flame volume of the helium-oxygen-acetylene flame, further underscores the sensitivity of that atom reservoir.

Signal-to-Noise Comparisons. Despite the increased fluorescence intensity produced by the helium-diluted flame, atomic fluorescence signal-to-noise ratios are no better than those produced by an air-supported flame. Table 4 compares signal-to-noise ratios for the helium-oxygen-acetylene, argon-oxygen-acetylene, and air-acetylene flames. Apparently, an increase in noise and a decrease in nebulization efficiency in the helium-diluted flame outweigh the signal gains. As a result, a poorer signal-to-noise ratio is found for this flame, relative to an air-acetylene flame. The argon-oxygen-acetylene flame of similar inert gas/oxygen ratio exhibits the same type of behavior (4).

The reduced signal-to-noise ratio obtained from the helium-oxygen-acetylene flame (cf. Table 4) can be attributed to increased flame emission which in turn results from the higher flame temperature. Johnson and Winefordner (4) improved signal-to-noise ratios in the argon-oxygen-acetylene flame by increasing the inert gas/oxygen ratio, which produced a lower flame temperature. Similar results would be expected for the helium-diluted flame, but were not verified in the present study.

Flame _Emission_ _Detection_ _Limits_. Although the increased temperature of the helium-oxygen-acetylene flame is a detriment to signal-to-noise ratios for fluorescence measurements, it is advantageous in flame emission. Flame emission detection limits, shown in Table 5, verify this expectation. Moreover, the increased fluorescence power efficiency in the He-fortified flame contributes to the improved emission sensitivity by decreasing the fraction of the excited state atoms that are quenched.

In Tables 4 and 5, calcium stands out as an element whose sensitivity is increased in _both_ fluorescence and emission measurements. This increase can be attributed entirely to the enhanced production of calcium atoms in the helium-diluted flame (2).

The improvements in emission detection limits for the helium-diluted flame listed in Table 5 correspond closely to increases in atomization efficiency by that flame (2). This atom formation efficiency is in the general order Ca>Ba>Sr>Cr>Fe>Cu. The same pattern is found in the emission detection limit study, except that Fe and Cr are switched in the order, because of increased noise at the wavelength of iron emission selected for this study.

The foregoing evaluation indicates that the instrumental system employed in this study is hardly optimal for exploiting fully the analytical capabilities of the helium-oxygen-acetylene flame. A number of improvements could be suggested and are being investigated in this laboratory. For example, changing the nebulization device employed in the system to yield equal sample delivery rates for all flame-gas mixtures would allow a more candid appraisal of the helium-diluted flame. In addition, the incorporation of a sheath-flame in place of the inert gas sheath might increase the fluorescence power efficiency. Nevertheless, the enhanced capabilities of the helium-oxygen-acetylene flame demonstrate that further investigation of this atom cell for atomic spectrometry is merited.

Appendix A. Determination of the Relative Detector Response Factor for the Atomic Fluorescence Power Efficiency Measurement System.

In the instrumental system employed for the measurement of atomic fluorescence power efficiencies, two monochromator-photomultiplier combinations were used to determine the intensity of radiant signals. Reference to the main text of this work shows that one detection combination was used in the measurement of fluorescence emitted by atoms in the flame, whereas the other combination was employed to determine energy absorbed by the atom cell. For the calculation of the atomic fluorescence power efficiency, the ratio of fluorescence radiance to absorbed radiance must be made, requiring a knowledge of the relative responsivity of the detection combinations.

Generally, the response, R, obtained from a detector placed at the exit slit of a monochromator when a continuum source of spectral radiance $B(\nu)$ in watts $cm^{-2}sr^{-1}nm^{-1}$ is incident upon the entrance slit is given by equation A-1 (21).

$$R = d\, B(\lambda)\, \tau W H \Omega S \qquad \text{(A-1)}$$

In the equation, d is the detector response factor which indicates the output current level per watt of radiant power incident on the device. W and H are the width and height of the monochromator entrance slit in cm; S is the spectral bandpass (in nm) for the selected slit width. The throughput of the monochromator is represented by τ, and the acceptance solid angle of the monochromator is Ω (in steradians). The equation assumes the source radiation completely fills the monochromator acceptance volume. If any external optics are incorporated into the system, τ will represent the combined throughput of both those optics and the monochromator.

When atomic fluorescence radiation is incident on the monochromator, the resulting detector response is given by:

$$I_F = d_F P_F \tau_F W_F H_F \Omega_F \qquad \text{(A-2)}$$

where P_F is the radiance of fluorescence in watts $cm^{-2} sr^{-1}$. Similarly, an absorption signal can be expressed:

$$\Delta I_A = d_A \Delta P_A \tau_A W_A H_A \Omega_A \qquad \text{(A-3)}$$

where ΔP_A is the radiance which is absorbed.

In the equation employed for the calculation of fluorescence power efficiencies (Eq. 1), the term $I_F/\Delta I_A$ appears, representing the ratio of the fluorescence to absorption signals from the photomultiplier. To correct for the detection system response, the correction factor D_F/D_A was applied such that:

$$\frac{I_F}{\Delta I_A} \cdot \frac{D_F}{D_A} = \frac{P_F}{\Delta P_A} \qquad \text{(A-4)}$$

From the above treatment, the ratio D_F/D_A can be shown to be equal to:

$$\frac{D_F}{D_A} = \frac{d_A\ \tau_A\ W_A\ H_A\ \Omega_A}{d_F\ \tau_F\ W_F\ H_F\ \Omega_F} \qquad \text{(A-5)}$$

To evaluate this system response factor, the monochromator and optical system specifications must be measured, in addition to the detector response factors, d_A and d_F.

Rather than evaluate each parameter in equation A-5, the combined effect of all the parameters was determined. The output of a continuum source was directed onto both the fluorescence and absorption monochromator entrance slits. The ratio of the detector responses measured in that experiment can be expressed by employing equation A-1 to obtain:

$$\frac{R_F}{R_A} = \frac{d_F\ \tau'_F\ W'_F\ H'_F\ \Omega'_F\ S'_F}{d_A\ \tau'_A\ W'_A\ H'_A\ \Omega'_A\ S'_A} \qquad \text{(A-6)}$$

where the primes designate the quantities used in the calibration procedure rather than the absorption or fluorescence signal detection experiment. If the same experimental conditions are used for both experiments, the combination of equations A-5 and A-6 yield:

$$\frac{D_F}{D_A} = \frac{R_A}{R_F} \cdot \frac{S_F}{S_A} \qquad \text{(A-7)}$$

The equation for the calculation of the power efficiency (Eq. 1) then becomes:

$$Y_P = \left(\frac{I_F}{\Delta I_A}\right)\left(\frac{W_A H_A}{W_F H_F}\right)\left(\frac{4\pi}{\Omega}\right)\left(\frac{A_F}{A_S}\right)\left(\frac{R_A}{R_F} \cdot \frac{S_F}{S_A}\right) \qquad \text{(A-8)}$$

The spectral slit width, S, is known to be equal to the product of the reciprocal linear dispersion of the monochromator, r, and the slit width, W, transforming equation A-8 to:

$$Y_P = \left(\frac{I_F}{\Delta I_A}\right)\left(\frac{H_A}{H_F}\right)\left(\frac{4\pi}{\Omega}\right)\left(\frac{A_F}{A_S}\right)\left(\frac{R_A}{R_F} \cdot \frac{r_F}{r_A}\right) \qquad \text{(A-9)}$$

Because two similar monochromators were used in this study, the reciprocal linear dispersions can be safely assumed to be equal. Also, the slit height for both monochromators was the same, leaving equation A-9 as:

$$Y_P = \left(\frac{I_F}{\Delta I_A}\right)\left(\frac{4\pi}{\Omega}\right)\left(\frac{A_F}{A_S}\right)\left(\frac{R_A}{R_F}\right) \qquad \text{(A-10)}$$

CREDIT

Supported in part by the National Science Foundation through grant CHE 77-22152 and by the Office of Naval Research. Taken in part from the Ph.D. thesis of K. A. Saturday.

LITERATURE CITED

1. K. A. Saturday and G. M. Hieftje, Anal. Chem., 49, 2015 (1977).

2. K. A. Saturday and G. M. Hieftje, Anal. Chem., submitted, 1979.

3. R. F. Browner, The Analyst (London), 99, 617 (1974).

4. D. J. Johnson and J. D. Winefordner, Anal. Chem., 48, 341 1976.

5. N. C. Clampitt and G. M. Hieftje, Anal. Chem., 46, 382 (1974).

6. D. R. Jenkins, Proc. Roy. Soc., Ser. A., 293, 493 (1966).

7. D. R. Jenkins, Proc. Roy. Soc., Ser. A., 303, 453 (1968).

8. D. R. Jenkins, Proc. Roy. Soc., Ser. A., 303, 467 (1968).

9. D. R. Jenkins, Proc. Roy. Soc., Ser. A., 306, 413 (1968).

10. K. M. Aldous, R. F. Browner, R. M. Dagnall and T. S. West, Anal. Chem., 42, 939 (1970).

11. J. A. Dean and T. C. Rains, "Standard Solutions for Flame Spectrometry" in "Flame Emission and Atomic Absorption Spectrometry", Vol. 2, J. A. Dean and T. C. Rains, Eds., Dekker, New York, 1971, Chapter 13.

12. S. J. Pearce, L. de Galan and J. D. Winefordner, Spectrochim. Acta, Part B, 23, 793 (1968).

13. H. P. Hooymayers and C. Th. J. Alkemade, J. Quant. Spectrosc. Radiat. Transfer, 6, 847 (1966).

14. H. P. Hooymayers and G. Nienhuis, *J. Quant. Spectrosc. Radiat. Transfer*, *8*, 955 (1968).

15. H. P. Hooymayers and P. L. Lijnse, *J. Quant. Spectrosc. Radiat. Transfer*, *9*, 995 (1969).

16. P. J. Th. Zeegers and J. D. Winefordner, *Spectrochim. Acta, Part B*, *26*, 161 (1971).

17. R. L. Cochran and G. M. Hieftje, *Anal. Chem.*, *49*, 2040 (1977).

18. P. A. St. John, W. J. McCarthy, and J. D. Winefordner, *Anal. Chem.*, *39*, 1495 (1967).

19. W. J. McCarthy, M. L. Parsons and J. D. Winefordner, *Spectrochim. Acta, Part B*, *23*, 25 (1967).

20. D. R. Jenkins, *Spectrochim. Acta, Part B*, *25*, 47 (1970).

21. H. T. Betz and G. L. Johnson, "Spectroradiometric Principles," in "Analytical Emission Spectroscopy," Chapter 5, Part 1, Dekker, New York (1971).

Table 1. Experimental Components and Conditions

Continuum Source	300 W Eimac illuminator with integral parabolic reflector; powered by a current-regulated power supply. (No. VIX-300UV, Varian Eimac Division, San Carlos, Calif.)
Chopper	480 Hz mechanical chopper (constructed in this laboratory) with associated lamp-phototransistor reference-signal generator.
Optics	L1, F.L. = 10.5 cm L2 and L3, F.L. = 8.5 cm All lenses are 3.8 cm diameter quartz. A 0.1% neutral-density filter, N. D. (Melles Griot, Danbury, Conn.) was placed at the entrance of the absorption monochromator. D_1 and D_2 are iris diaphragms (1.25, 0.90 cm diameter, respectively).

Burner	Capillary burner with an inert gas sheath and interchangeable burner heads for the helium-oxygen-acetylene and air-acetylene mixtures (see text for further details.)
Nebulizer	Impingement bead-type premix nebulizer chamber (Model No. 25958) with concentric pneumatic nebulizer (Model No. 20851-01, Instrumentation Laboratories, Inc., Lexington, Mass.)
Gas Handling System	Described previously (1).
Gas Flow Rates	1.9 L/min acetylene used throughout. Air/Acetylene flame: 10.8 L/min air with 5.0 L/min nitrogen sheath Helium-oxygen-acetylene flame: 8.4 L/min helium 2.4 L/min oxygen with 3.2 L/min helium sheath

Monochromators	Absorption: Digital step-scanning monochromator (Model EU-700) with associated controller (Model EU-700-32, GCA/McPherson Instruments, Acton, Mass.) Fluorescence: Monochromator with programmable filter attachment (Model EU-700-55, GCA/McPherson Instrument, Acton, Mass.) Both monochromators are 0.35 m f/6.8 Czerny-Turner mounts with 48 x 48 mm gratings and reciprocal linear dispersion of 20 Å/mm.
Detectors	Absorption: RCA#1P28 photomultiplier was contained in a Model 50B housing (Pacific Photometric Instruments, Emeryville, Calif.) powered at -700V with a high voltage supply (Model EU-42A, Heath Co., Benton Harbor, MI) Fluorescence: An R446 photomultiplier (Hamamatsu Corp., Middlesex, N.J.) was contained in a Model 3150 housing (Pacific Photometric Instruments, Emery-

	ville, Calif.) powered at -1000V with a high voltage supply (Model 244, Keithley Instruments, Inc., Cleveland, Ohio).
Signal Processing	The photocurrent was amplified (Model 427, Keithley Instruments Inc., Cleveland, Ohio) and converted to a proportional voltage before being processed by a lock-in amplifier (Model 128, Princeton Applied Research Corp., Princeton, N. J.).
Readout Devices	The resulting signals could be observed with a strip chart recorder (Model EU-205-11 with Model EU-200-01 potentometric amplifier and Model EU-200-02 offset module, Heath-Schlumberger, Benton Harbor, Mi.) or an integrating digital voltmeter (Model 5326B, Hewlett-Packard, Palo Alto, Calif.).

Table 2. Evaluated Experimental Constants for Equation (1).

Parameter	Value
H_F, H_A	5mm
W_A/W_F	5.4
Ω	0.021 sterad
A_F	1.0 cm^2 air/acetylene flame 1.5 cm^2 $He/O_2/C_2H_2$ flame
A_S	0.48 cm^2

Subscripts A and F denote absorption and fluorescence, respectively.

H_A, H_F = height of monochromator entrance slit

W_A, W_F = width of monochromator entrance slit

Ω = solid angle of fluorescence radiation collected

A_F = fluorescent area in flame

A_S = area of image at absorption monochromator entrance slit

Table 3. Fluorescence power efficiencies for the air-acetylene and helium-oxygen-acetylene flames.

Element	Wavelength (nm)	Neutral Density Filter Transmission (%T)[c]	Concentration Range ($\mu g\ mL^{-1}$)	Y_p[a]		
				Air/Acetylene	$He/O_2/C_2H_2$	Ratio[b]
Fe	248.2	0.0269	100-500	0.31	0.71	2.3
Mg	285.2	0.117	2-30	0.13	0.38	2.9
Cu	324.7	0.170	30-100	0.049	0.14	2.9
Cr	357.9	0.186	300-600	0.061	0.35	5.7
Ca	422.7	0.355	10-75	0.19	0.67	3.5

(a) The average relative standard deviation in the fluorescence power efficiencies, Y_p. were ±10%, obtained from three determinations.

(b) The power efficiencies in $He/O_2/C_2H_2$ are ratioed to those in the air-acetylene flame.

(c) See Figure 1.

Table 4. Signal-to-noise ratio comparison between air-C_2H_2, He-O_2-C_2H_2 and Ar-O_2-C_2H_2 flames.

Element	$(S/N)^a_{He}/(S/N)_{air}$	$(S/N)_{Ar}/(S/N)^b_{air}$
Zn	0.28	0.71
Fe	0.11	0.60
Mg	0.34	0.55
Cu	0.43	0.40
Cr	0.46	1.4
Ca	1.85	-

(a) Subscripts: He refers to the He-O_2-C_2H_2 flame; air denotes the air-C_2H_2 flame; and Ar indicates the Ar-O_2-C_2H_2 flame.

(b) From Ref. (4). The Ar/O_2 ratio for these measurement was similar to the He/O_2 ratio employed in the present work.

Table 5. Flame Emission Detection Limits

Element	Wavelength (nm)	Detection Limit (μg/mL)		
		Air/C_2H_2	He/O_2/C_2H_2	Ratio
Cu	324.7	7.21	1.87	3.86
Fe	372.0	22.7	7.74	2.93
Mn	403.1	2.95	1.12	2.63
Ca	422.7	0.85	0.079	10.71
Cr	425.4	4.00	0.91	4.40
Sr	460.7	0.74	0.086	8.62

FIGURE CAPTIONS

Figure 1. Schematic diagram of the optical system used for determination of fluorescence power efficiencies. Details concerning the experimental components can be found in Table 1, and a discussion of the apparatus is contained in the text.

Figure 2. Fluorescence growth curve for copper (324.7 nm).

A. Helium-oxygen-acetylene flame.

B. Air-Acetylene flame.

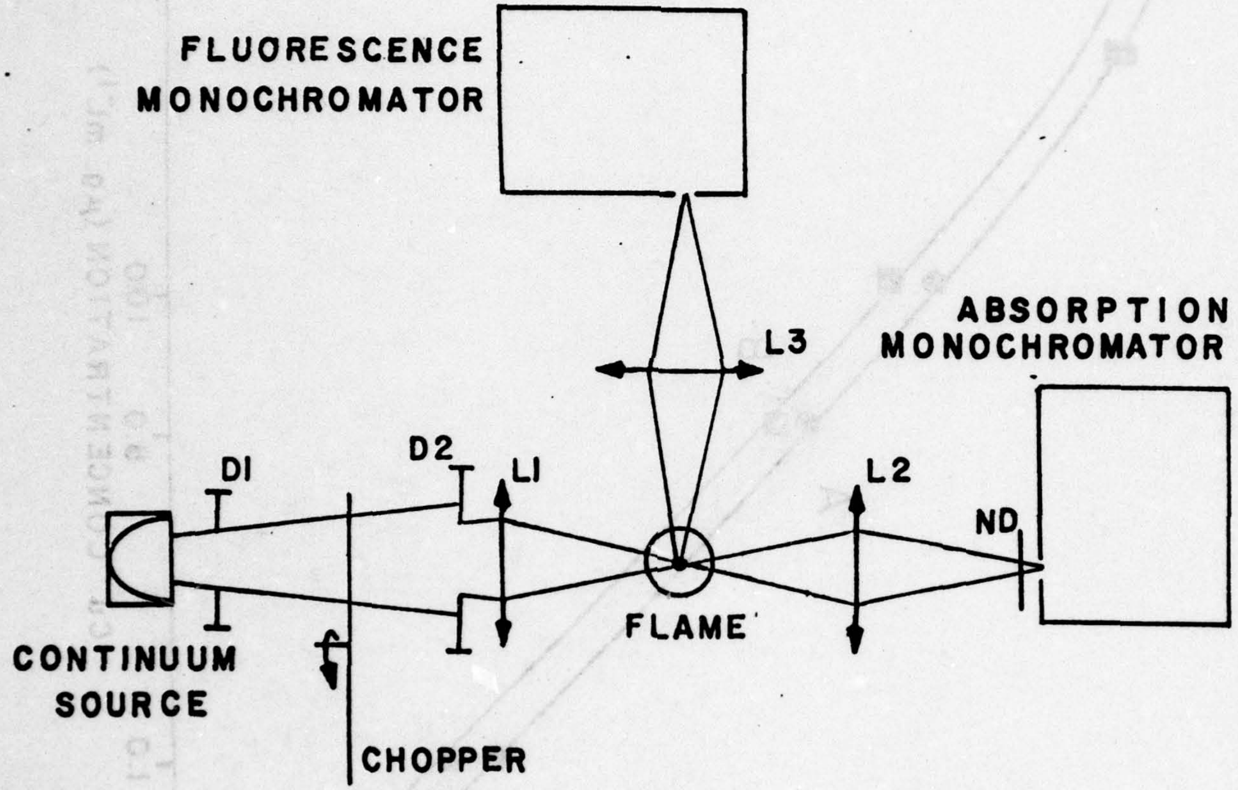
FLUORESCENCE
MONOCHROMATOR
L3
ABSORPTION
MONOCHROMATOR
DI
D2
LI
L2
ND
CONTINUUM
SOURCE
FLAME
CHOPPER

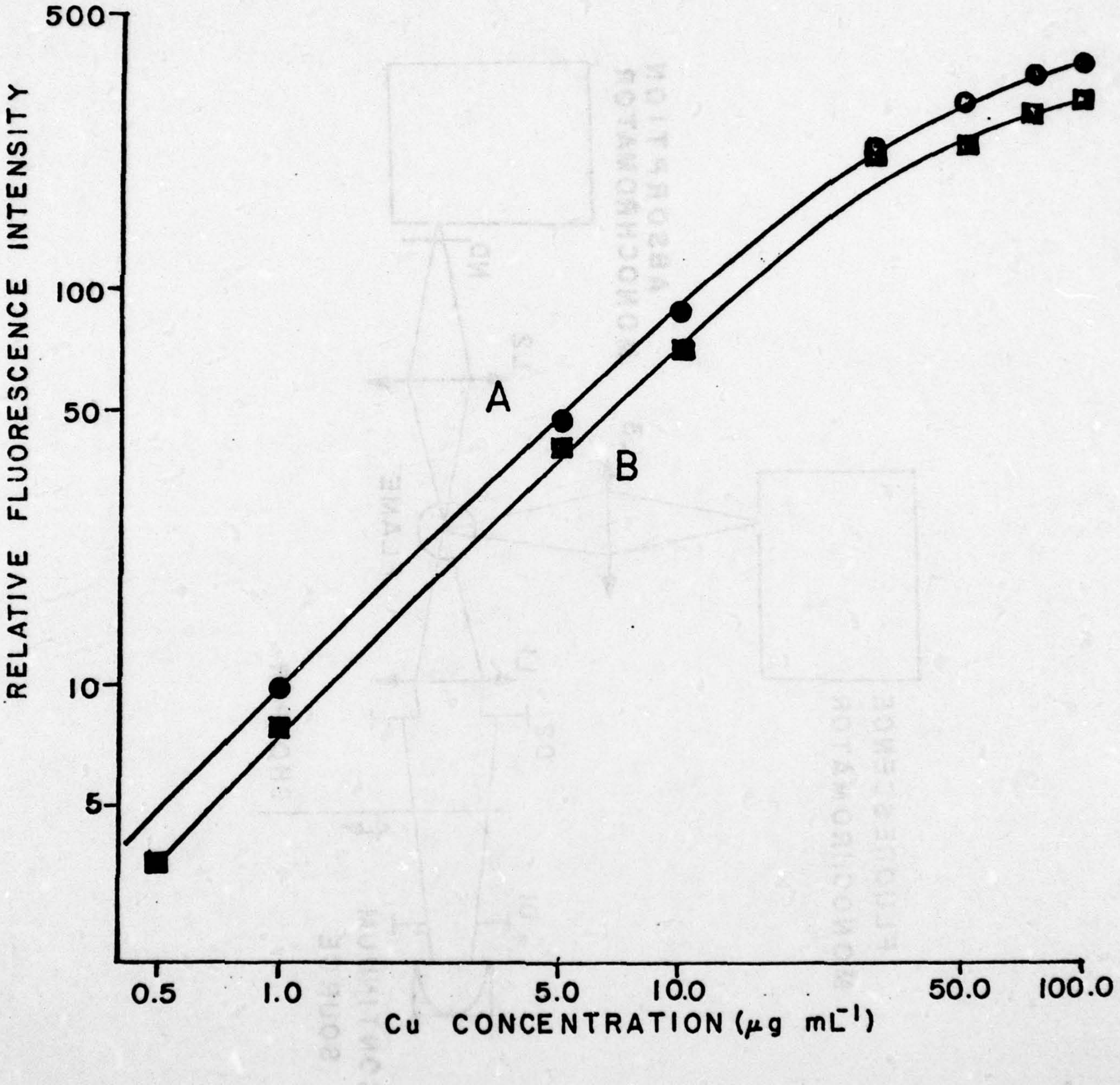
500
100
50
10
5
RELATIVE FLUORESCENCE INTENSITY
A
B
0.5
1.0
5.0
10.0
50.0
100.0
Cu CONCENTRATION (μg mL⁻¹)

TECHNICAL REPORT DISTRIBUTION LIST, GEN

No. Copies

Office of Naval Research
800 North Quincy Street
Arlington, Virginia 22217
Attn: Code 472 2

ONR Branch Office
536 S. Clark Street
Chicago, Illinois 60605
Attn: Dr. George Sandoz 1

ONR Branch Office
715 Broadway
New York, New York 10003
Attn: Scientific Dept. 1

ONR Branch Office
1030 East Green Street
Pasadena, California 91106
Attn: Dr. R. J. Marcus 1

ONR Area Office
One Hallidie Plaza, Suite 601
San Francisco, California 94102
Attn: Dr. P. A. Miller 1

ONR Branch Office
Building 114, Section D
666 Summer Street
Boston, Massachusetts 02210
Attn: Dr. L. H. Peebles 1

Director, Naval Research Laboratory
Washington, D.C. 20390
Attn: Code 6100 1

The Assistant Secretary
of the Navy (R,E&S)
Department of the Navy
Room 4E736, Pentagon
Washington, D.C. 20350 1

Commander, Naval Air Systems Command
Department of the Navy
Washington, D.C. 20360
Attn: Code 310C (H. Rosenwasser) 1

No. Copies

Defense Documentation Center
Building 5, Cameron Station
Alexandria, Virginia 22314 12

U.S. Army Research Office
P.O. Box 1211
Research Triangle Park, N.C. 27709
Attn: CRD-AA-IP 1

Naval Ocean Systems Center
San Diego, California 92152
Attn: Mr. Joe McCartney 1

Naval Weapons Center
China Lake, California 93555
Attn: Dr. A. B. Amster
Chemistry Division 1

Naval Civil Engineering Laboratory
Port Hueneme, California 93401
Attn: Dr. R. W. Drisko 1

Professor K. E. Woehler
Department of Physics & Chemistry
Naval Postgraduate School
Monterey, California 93940 1

Dr. A. L. Slafkosky
Scientific Advisor
Commandant of the Marine Corps
(Code RD-1)
Washington, D.C. 20380 1

Office of Naval Research
800 N. Quincy Street
Arlington, Virginia 22217
Attn: Dr. Richard S. Miller 1

Naval Ship Research and Development
Center
Annapolis, Maryland 21401
Attn: Dr. G. Bosmajian
Applied Chemistry Division 1

Naval Ocean Systems Center
San Diego, California 91232
Attn: Dr. S. Yamamoto, Marine
Sciences Division 1

Encl 1

TECHNICAL REPORT DISTRIBUTION LIST, 051C

	No. Copies
Dr. M. B. Denton University of Arizona Department of Chemistry Tucson, Arizona 85721	1
Dr. R. A. Osteryoung Colorado State University Department of Chemistry Fort Collins, Colorado 80521	1
Dr. B. R. Kowalski University of Washington Department of Chemistry Seattle, Washington 98105	1
Dr. S. P. Perone Purdue University Department of Chemistry Lafayette, Indiana 47907	1
Dr. D. L. Venezky Naval Research Laboratory Code 6130 Washington, D.C. 20375	1
Dr. H. Freiser University of Arizona Department of Chemistry Tuscon, Arizona 85721	
Dr. Fred Saalfeld Naval Research Laboratory Code 6110 Washington, D.C. 20375	1
Dr. H. Chernoff Massachusetts Institute of Technology Department of Mathematics Cambridge, Massachusetts 02139	1
Dr. K. Wilson University of California, San Diego Department of Chemistry La Jolla, California 92037	1
Dr. A. Zirino Naval Undersea Center San Diego, California 92132	1
Dr. John Duffin United States Naval Postgraduate School Monterey, California 93940	1
~~Dr. G. M. Hieftje~~ ~~Department of Chemistry~~ ~~Indiana University~~ Bloomington, Indiana 47401	1
Dr. Victor L. Rehn Naval Weapons Center Code 3813 China Lake, California 93555	1
Dr. Christie G. Enke Michigan State University Department of Chemistry East Lansing, Michigan 48824	1
Dr. Kent Eisentraut, MBT Air Force Materials Laboratory Wright-Patterson AFB, Ohio 45433	1
Walter G. Cox, Code 3632 Naval Underwater Systems Center Building 148 Newport, Rhode Island 02840	1

Encl 1